JOURNAL OF TISSUE ENGINEERING AND REGENERATIVE MEDICINE
J Tissue Eng Regen Med 2016.
Published online in Wiley Online Library (wileyonlinelibrary.com) **DOI:** 10.1002/term.2167

RESEARCH ARTICLE

Low oxygen tension reveals distinct *HOX* codes in human cord blood-derived stromal cells associated with specific endochondral ossification capacities *in vitro* and *in vivo*

Stefanie Liedtke[1]*, Benedetto Sacchetti[2], Anita Laitinen[3], Samantha Donsante[2], Robert Klöckers[1], Saara Laitinen[3], Mara Riminucci[2] and Gesine Kogler[1]

[1]*Institute of Transplantation Diagnostics and Cell Therapeutics, Heinrich-Heine-University Medical Centre, Düsseldorf, Germany*
[2]*Stem Cell Laboratory, Department of Molecular Medicine, Sapienza University, Rome, Italy*
[3]*Research and Development, Medical Services, Finnish Red Cross Blood Service, Helsinki, Finland*

Abstract

Effects of oxygen tension on the generation, expansion, proliferation and differentiation of stromal cell types is widely described in the literature. However, data on the internal heterogeneity of applied cell populations at different O_2 levels and possible impacts on differentiation potentials are controversial. Here, the expression of 39 human *HOX* genes was determined in neonatal cord blood stromal cells and linked to differentiation-associated signatures. In cord blood, unrestricted somatic stromal cells (USSCs), lacking *HOX* gene expression, and cord blood-derived multipotent stromal cells (CB-MSCs), expressing about 20 *HOX* genes, are distinguished by their specific *HOX* code. Interestingly, 74% of the clones generated at 21% O_2 were *HOX*-negative USSCs, whereas 73% of upcoming clones at 3% O_2 were *HOX*-positive CB-MSCs. In order to better categorize distinct cell lines generated at 3% O_2, the expression of all 39 *HOX* genes within *HOX* clusters A, B, C and D were tested and new subtypes defined: cells negative in all four *HOX* clusters (USSCs); cells positive in all four clusters (CB-MSCs^{ABCD}); and subpopulations missing a single cluster (CB-MSCs^{ACD} and CB-MSCs^{BCD}). Comprehensive qPCR analyses of established chondro-osteomarkers revealed subtype-specific signatures verifiably associated with *in vitro* and *in vivo* differentiation capacity. The data presented here underline the necessity of better characterizing distinct cell populations at a clonal level, taking advantage of the inherent specific *HOX* code as a distinguishing feature between individual subtypes. Moreover, the correlation of subtype-specific molecular signatures with *in vitro* and *in vivo* bone formation is discussed. Copyright © 2016 John Wiley & Sons, Ltd.

Received 1 September 2015; Revised 21 December 2015; Accepted 3 February 2016

Keywords **USSCs; CB-MSCs; BM-MSCs; *HOX* code; *in vivo* bone; chondrogenesis; osteogenesis; endochondral signature**

1. Introduction

There is an increasing need to reproducibly regenerate cartilage and bone and, to date, various cell-based clinical approaches have been investigated, mainly demonstrating crude immunophenotype and artificial *in vitro* differentiation assays without *in vivo* confirmation. Moreover, a comprehensive molecular characterization of applied cell types is hampered by the strong heterogeneity of individual cell lines (Harrington *et al.*, 2014) and strong overlap of surface marker expression profiles (Busser *et al.*, 2015). In addition, most results have not been produced at a clonal level and uncertainties remain with respect to the defining characteristics of these cells (Bianco *et al.*, 2008).

In 2004, a cord blood-derived stromal cell type, named unrestricted somatic stromal cells (USSCs), was isolated

**Correspondence to: S. Liedtke, Institute for Transplantation Diagnostics and Cell Therapeutics, Heinrich-Heine-University Medical Centre, Moorenstrasse 5, D-40225 Düsseldorf, Germany. E-mail: Stefanie.Liedtke@med.uni-duesseldorf.de*

from cord blood (CB) and described as a homogeneous cell population revealing a bone marrow stroma cells (BM-MSC)-like immunophenotype (Kogler *et al.*, 2004). During the last decade, further detailed characterization *in vitro* and *in vivo*, applying clonal cell populations, clearly revealed at least two distinct cell populations, named USSCs and cord blood multipotent stromal cells (CB-MSCs; also called cord blood-derived stromal cells, CDSCs), according to the revisited MSC concept (Bianco *et al.*, 2008). Clonal USSCs and CB-MSCs lines differ most likely in their developmental origin, reflected by a distinct *HOX* (homeobox) gene expression pattern (Liedtke *et al.*, 2010) and expression of the Delta-like 1 homologue (*DLK1*) (Kluth *et al.*, 2010), manifesting distinct differentiation capacities (Bosch *et al.*, 2012).

Besides adult BM-MSCs, neonatal cord blood USSCs and CB-MSCs are attractive cell sources for bone-regenerative approaches *in vivo* (Handschel *et al.*, 2010; Klontzas *et al.*, 2015; Langenbach *et al.*, 2011). Like the 'gold standard' BM-MSCs, neonatal cord blood-derived USSCs and CB-MSCs can be differentiated *in vitro* into the chondrogenic and osteogenic lineages, while showing a more immature osteogenic signature in comparison to adult BM-MSCs (Bosch *et al.*, 2013). These cell type-associated signatures may be correlated with the specific expression of *HOX* genes.

In the human system, 39 *HOX* genes, located in four distinct clusters, A, B, C and D, are distributed among chromosomes 7 (11 HOXA genes), 17 (10 HOXB genes), 12 (nine HOXC genes) and 2 (nine HOXD genes) (Krumlauf, 1994). While the establishment of tightly regulated *HOX* expression patterns is important for developing limbs during embryonic and fetal development (Izpisua-Belmonte and Duboule, 1992), specific *HOX* codes are maintained in adult cells, such as fibroblasts (Chang *et al.*, 2002), mesenchymal stromal cells (Ackema and Charite, 2008) and osteoprogenitor cells (Leucht *et al.*, 2008). Ackema and Charite (2008) described characteristic topographic *HOX* codes in murine mesenchymal stromal cells from different anatomical sites. In line with this, our group determined the specific *HOX* code in human adult and neonatal cord blood stromal cell types revealing *HOX* expression in all four clusters in adult BM-MSCs similar to neonatal CB-MSCs, whereas USSCs display absent or only marginal *HOX* expression (Liedtke *et al.*, 2010).

USSCs and CB-MSCs derived from cord blood must be clearly distinguished from stromal cells derived from umbilical cord (UC-MSCs), since UC-MSCs fail to differentiate *in vitro* and *in vivo* (Kaltz *et al.*, 2008; Reinisch *et al.*, 2015), differ in their typical *HOX* expression pattern, and have a different molecular chondro-osteogenic signature lacking relevant integrin-binding sialoprotein (*IBSP*) expression (Bosch *et al.*, 2012). *HOX* genes are known to be involved in cartilage formation (Goldring *et al.*, 2006) and the transcriptional control of skeletogenesis (Karsenty, 2008). With regard to bone-regenerative approaches, it is therefore promising to characterize the individual inherent *HOX* code of potential cell sources linked to their inherent chondro-osteogenic potential. The distinct embryonic origin reflected by the topographic *HOX* code might additionally have an impact on regenerative approaches with regard to the inherent skeletogenic potential of a cell (Leucht *et al.*, 2008). The heterogeneity among different or even the same cell sources is obvious, but not easy to resolve (McKenna *et al.*, 2015; Viswanathan *et al.*, 2015). Not only the source-dependent and donor-dependent heterogeneity of individual cell types (Wegmeyer *et al.*, 2013) but also the additional impact of low oxygen conditions on distinct cell types must be elucidated, as cells that are transplanted into injured tissues constantly encounter hypoxic stress.

This study emphasizes elucidation of the generation frequency and distribution of human cord blood-derived stromal cell types, comparing normoxia (21% O_2) with low oxygen tension (3% O_2). Moreover, new cord blood-derived subtypes are introduced, characterized by their inherent *HOX* codes. Besides the classification of stromal cell subtypes based on their specific *HOX* expression patterns, individual molecular signatures of neonatal cord blood stromal cell subtypes involved in cartilage and bone regeneration are described here. Finally, the interrelation between the inherent *HOX* code, endochondral molecular signature and *in vitro* and *in vivo* differentiation capacity is presented.

2. Materials and methods

2.1. Generation and expansion of USSCs, CB-MSCs and BM-MSCs

Neonatal cord blood stromal cells were generated as described previously, either at 21% O_2 (Kogler *et al.*, 2004) or at 3% O_2 (Laitinen *et al.*, 2011). For culture, 5–7 $\times$ 10^6 cells/ml were loaded into T75 culture flasks (Corning) in Dulbecco's modified eagle's medium (DMEM) low-glucose (Cambrex) with 30% fetal bovine serum (FCS; Perbio), penicillin–streptomycin and L-glutamine (PSG; Cambrex) and cultivated for at least two further passages. Samples were collected in accordance with the Declaration of Helsinki, after written informed consent. The ethical approval to isolate the respective cell types was obtained from the ethical review board of the Medical Faculty, University of Duesseldorf (USSCs/CB-MSCs: Study No. 2975) or approved by the ethical review board of Helsinki University Central Hospital and the Finnish Red Cross Blood Service. Clonal populations were obtained by applying special cloning cylinders (Chemicon, Billerica, MA, USA), as described earlier (Kluth *et al.*, 2010). Bone marrow was directly plated for the generation of MSCs in DMEM low-glucose with 30% FCS and PSG until adherent colonies appeared. All neonatal cord-blood derived cell types were cultured

DOI: 10.1002/term

at either 3% or 21% O_2 at 37°C in a humidified atmosphere with 5% CO_2 until reaching 80% confluence in DMEM low-glucose with 30% FCS and PSG (Kogler *et al.*, 2004). All stromal cell lines were detached with 0.25% trypsin.

Isolation and generation of cells from the umbilical cord (UC), applied as a negative control here (Figure 6), were performed as described previously (Bosch *et al.*, 2012).

2.2. *In vitro* differentiation

All stromal cell lines were differentiated as described previously, under normoxic conditions (Bosch *et al.*, 2012). In brief, for osteogenic differentiation, induction was performed in DMEM low-glucose medium with 30% FCS, PSG, 10^{-7} M dexamethasone, 50 mg/ml ascorbic acid 2-phosphate and 10 mM β-glycerol-phosphate (all from Sigma-Aldrich) and changed twice weekly over a total run time of 14 days. After 14 days of osteogenic differentiation, mineralization was detected by alizarin red S staining (Sigma-Aldrich) as well as with more sensitive von Kossa staining (silver nitrate 5%; Roth), according to standard protocols.

Chondrogenesis was performed in a 3D pellet culture system and the pelleted cells were incubated for 21 days in DMEM high-glucose with PSG, 100 nM dexamethasone, 35 mg/ml ascorbic acid-2-phosphate, 1 mM sodium pyruvate (all Sigma-Aldrich), insulin–transferrin–selenium (1/100 dilution; Gibco, Invitrogen) and 10 ng/ml TGFβ1 (MACS; Miltenyi Biotec). The medium was changed twice weekly.

After 21 days of chondrogenic differentiation, pellets were embedded in Tissue Freezing Medium (Jung, Leica) and cut into sections of 10 mm using a cryotome. The areas and diameters of the pellets were measured at days 7, 14 and 21, using AVISO CellCelector analySIS image software. For each time point, $n = 5$ pellets were measured, and the arithmetic mean and standard deviation (SD) were calculated (see supporting information, Figure S4). Safranin O (Waldeck) staining was applied for the detection of proteoglycan content in normal cartilage counterstained with Fast Green (Sigma), following a standard protocol.

2.3. *In vivo* transplantation assays

2.3.1. Heterotopic bone formation

To assess osteogenic potential, constructs of test cells and osteoconductive material (hydroxyapatite–tricalcium phosphate particles, HA/TCP) was performed as reported (Krebsbach *et al.*, 1997; Sacchetti *et al.*, 2007). All animal procedures were approved by the relevant institutional committee. Cells (2×10^6) were allowed to attach to hydroxyapatite–tricalcium phosphate particles (40 mg, 100–200 μm; Zimmer, Warsaw IN, USA) and embedded in a fibrin gel. The carrier–cell constructs were transplanted subcutaneously in the backs of 6–15 week-old female *xid/bg* mice (CB17.Cg-Prkdcscid Lystbg/Crl; Charles River Laboratories International, Wilmington, MA, USA).

2.3.2. Histology

Heterotopic transplants were harvested at 8 weeks, fixed in 4% formaldehyde in phosphate buffer, decalcified in 10% EDTA and processed for paraffin embedding. Sections 5 μm thick were stained with haematoxylin and eosin (H&E; Sigma) for histology. Brightfield and polarized light microscopy images were obtained using a Zeiss Axiophot microscope (Carl Zeiss, Germany).

2.4. Total RNA extraction and reverse transcription

Total RNA was extracted from cell lines in a 40 μl volume, applying the RNeasy Kit (Qiagen), according to the manufacturer's instructions, including the optional 15 min DNAse digest. Determination of RNA concentrations and purity was carried out by applying a Nanodrop device (NanoDropTechnologies).

Reverse transcription was performed using the First-strand cDNA Synthesis Kit (Invitrogen) and oligo(dT) 20 primer (ThermoScientific), following the manufacturer's instructions. About 1000 ng total RNA was converted into first-strand cDNA in a 20 μl reaction.

2.5. RT–PCR (determination of *HOX* expression pattern)

HOX expression patterns of all cell lines, generated and cultivated at either 21% or 3% O_2, were tested (see supporting information, Figure S1). RT–PCR was carried out with intron-spanning primers specific for each *HOX* gene (Liedtke *et al.*, 2010, 2013) (Thermo Scientific); the respective primer sequences are given in Table S2 (see supporting information) and *GAPDH* was used as the reference gene. Approximately 50 ng cDNA was used for subsequent RT–PCR analysis in a total volume of 25 μl containing 1× PCR buffer, 0.2 μM each primer, 0.75 mM $MgCl_2$, 0.2 mM each dNTP and 1 U *Taq* DNA Polymerase (Invitrogen) under the following conditions: (a) 2 min at 95°C for initial denaturation; (b) 30 s at 95°C, 30 s at 56°C; (c) 30 s at 72°C for 35 cycles; (d) 5 min at 72°C for final extension of the PCR products. PCR was performed on a Mastercycler ep gradient S (Eppendorf). Subsequently, aliquots of the RT–PCR products and related controls were analysed by electrophoresis on a 2% agarose gel containing Midori green (Biozym Scientific).

DOI: 10.1002/term

2.6. qPCR (determination of differentiation-specific markers)

Quantitative PCR (qPCR) was carried out with intron-spanning primers specific for each gene (Thermo Scientific). The sequences for primers (see supporting information, Table S1) were carefully examined and checked for their specificity by applying BLASTn; *RPL13A* was used as the reference gene for normalization. qPCR was carried out with SYBR® Green PCR Mastermix (Applied Biosystems). All reactions were run in technical triplicates with $n = 3$ biological correlates, respectively, on a Step One Plus (Applied Biosystems) instrument. The PCR reactions had a total volume of 25 µl, containing 12.5 µl Power SYBR® Green PCR, 6 µl distilled water, 2.5 µl (10 ng) template and 4 µl (0.2 µM) each primer. The PCR parameters were (10 min at 95°C, followed by 15 s at 95°C and 1 min at 60°C) for 35 cycles. To run and analyse the comparative *C*T experiments, Step One software v. 2.1 was used. The threshold was fixed at 0.2 for all experiments. Relative changes in gene expression were calculated by applying the comparative *C*T method (Schmittgen and Livak, 2008). The 2^{-C}T fold change of the internal control *RPL13A* in 3% O_2 samples vs 21% O_2 controls was 1.01 ($1.72^{-5}/1.70^{-5}$), qualifying *RPL13A* as a stable internal control. Differential gene expression was calculated by the formula $2^{-\Delta C}$T related to *RPL13A* or $2^{-\Delta\Delta C}$T normalized to BM-MSCs ($n = 3$). Fold changes <1 were transformed by the formula $-1/2^{-\Delta\Delta C}$T in the case of downregulated genes and plotted together with positive fold changes and upregulated genes, respectively (Figure 4). Data are presented as arithmetic means with standard error (SE) of the mean.

3. Results

3.1. Cloning-efficiency of CB-derived cell lines generated at 3% vs 21% O_2

In order to determine an accurate generation frequency comparing low oxygen tension (3% O_2) vs normoxia (21% O_2), mononuclear cells (MNCs) from 24 individual cord blood units were divided into equal volumes and seeded simultaneously under 21% and 3% O_2 conditions. Primary colonies could be obtained from 12/24 samples (50%) with a mean of 2.4 ± 2.19 clones at 21% O_2/CB sample and 3.9 ± 2.5 clones at 3% O_2/CB sample. A higher abundance of colonies was found at 3% O_2 in 11/24 CB samples in comparison to 5/24 CB samples generated at 21% O_2 (Figure 1A). In seven of 24 CB samples (29%), clones could be harvested exclusively from 3% O_2, compared to only one single CB (4%), revealing clones exclusively at 21% O_2. In 4/24 (17%) CB samples colonies were detected in both the 21% and 3% O_2 flasks. Low oxygen tension therefore leads to a significantly higher cloning efficiency than normoxia.

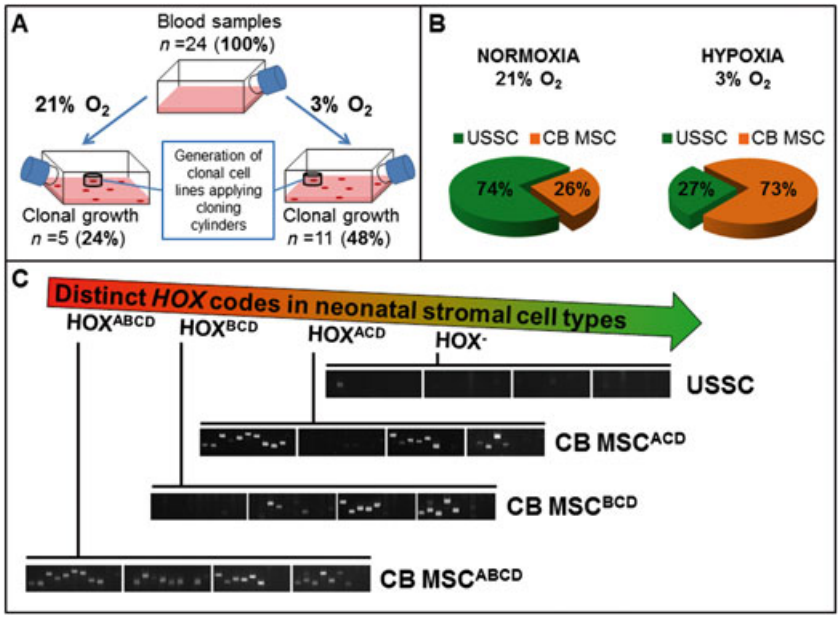

Figure 1. Cloning efficiency and distribution of neonatal cord blood cell types at 21% vs 3% O_2. (A) Cloning efficiency of cord blood samples generated at 21% O_2 normoxia vs 3% O_2; from 24 individual cord blood units, MNC fractions were divided into equal portions and seeded at either 21% or 3% O_2 conditions. (B) The expression of 39 *HOX* genes was tested by RT–PCR in $n = 50$ cell lines generated and cultivated at normoxia (21% O_2) and $n = 15$ cell lines generated and cultivated at low oxygen tension (3% O_2). The percentage of *HOX*-negative USSCs and *HOX*-positive CB-MSC^{ABCD} shifts at 3% O_2, revealing a prevalence of *HOX*-positive subtypes. (C) Categorization of neonatal cord blood subpopulations based on *HOX* expression pattern: four subtypes were defined by the cluster-specific expression of *HOX* genes; expression in clusters ABCD, or BCD, or ACD (CB-MSC subtype) or no expression in any cluster (USSC subtype) was determined and the cell lines were grouped

DOI: 10.1002/term

3.2. Distribution of HOX expression patterns under 3% vs 21% O_2 conditions and definition of subtypes

In total, $n = 50$ individual cell lines generated at 21% O_2 have so far been tested for their specific *HOX* codes in our laboratory (data not shown). Interestingly, the distribution of stromal subtypes characterized by distinct *HOX* expression patterns was dependent on the oxygen tension (Figure 1B). At 21% O_2, 37/50 (74%) cell lines tested revealed no or only marginal expression of *HOX* genes in any cluster, defining them as bona fide USSCs, whereas 13/50 (26%) were *HOX*-positive CB-MSCs [three of 13 (23%) *HOX*-positive lines with lack of expression within the HOXB cluster, viz. CB-MSCs^{ACD}]. Therefore, USSCs are the main neonatal cord blood cell type obtained at normoxia. At 3% O_2, this distribution switches; from 15 cell lines generated under low-O_2 conditions, only four (27%) revealed an USSCs subtype without expression of *HOX* genes and 11 (73%) cell lines revealed *HOX* expression according to the CB-MSCs subtype. This supposes that 3% O_2 leads to a preferential colony growth of *HOX*-positive subtypes, independent of the collection centre generating the cell lines (data not shown). However, from the 11 cell lines positive for *HOX*-expression at 3% O_2, five of 11 (46%) lines revealed a lack of gene expression within the HOXB cluster (CB-MSCs^{ACD}) and one cell line missed the HOXA cluster (CB-MSCs^{BCD}). The cellular subtype missing the HOXB cluster seemed to be preferred at 3% O_2. Finally, the resulting cell populations were categorized into four main cellular subtypes (Figure 1C), based on their *HOX* codes (see supporting information, Figure S1). Defined groups were *HOX*-negative USSCs and three categories of *HOX*-positive CB-MSCs, showing expression either in all four *HOX* clusters (CB-MSCs^{ABCD}), or expression in *HOX* clusters B, C and D (CB-MSCs^{BCD}), or in *HOX* clusters A, C and D (CB-MSCs^{ACD}). Adult BM-MSC control cells ($n = 3$) always showed expression in all four *HOX* clusters without exception (see supporting information, Figure S1A).

3.3. Expression of chondrogenic markers in distinct subtypes

In order to determine whether defined subtypes of cells reveal a distinct basic expression of chondrogenesis-associated markers (Figure 2), the following genes were tested by qPCR: *COL1A1* (collagen, type I α1); *COL2A1* (collagen, type II α1); *COL10A1* (collagen, type X α1); *FOSL2* (FOS-like antigen 2); *PTHLH* (parathyroid hormone-like hormone); *WNT9A* (wingless-type MMTV integration site family, member 9 A); *WNT10B* (wingless-type MMTV integration site family, member 10B); and *ACAN* (aggrecan).

3.3.1. Differences at 21% O_2 (Figure S2)

Normoxic USSCs ($n = 3$), CB-MSCs^{ABCD} ($n = 3$) and BM-MSCs ($n = 3$) lines revealed significant differences for *COL10A1*, highest in adult normoxic BM-MSCs compared to neonatal normoxic USSCs and CB-MSCs^{ABCD} (Figure S2), whereas *COL1A1* and *COL2A1* expression was detected at a similar expression level. *ACAN* was highly expressed in CB-MSCs^{ABCD} in comparison with USSCs and BM-MSCs, revealing comparable lower expression levels.

3.3.2. Differences at 3% O_2 (Figure S2)

Significant upregulation was detected in CB-MSCs^{ABCD} at 3% O_2 for *COL1A1*, *COL2A1* and *WNT9A*. However, higher expression of the same genes in USSCs at 3% O_2 vs USSCs at 21% O_2 was not significant, due to biological variances between single clonal cell lines. The late chondrogenic marker *ACAN* was already higher in CB-MSCs^{ABCD} at normoxia and further increased upon 3% O_2, whereas USSCs revealed a lower expression at 3% O_2, suggesting a distinct kind of regulation between *HOX*-positive and *HOX*-negative subtypes. In general, the basic expression levels of chondrogenic markers were higher in CB-MSCs^{ACD} subtype vs CB-MSCs^{BCD} subtype, except for the early marker *COL1A1*, revealing the lowest expression in CB-MSCs^{ACD} subtype and *WNT9A* showing a similar expression level. Expression of the later chondrogenic marker *COL10A1* was highest in CB-MSCs-^{ACD} subtype.

3.4. Expression of osteogenic markers in distinct subtypes

Basic expression of genes involved in osteogenic differentiation (Figure 3) was determined for: *IBSP/BSP* (integrin-binding sialoprotein); *BMP2* (bone morphogenetic protein 2); *BMP4* (bone morphogenetic protein 4); *BGLAP/OC* [bone γ-carboxyglutamate (gla) protein/osteocalcin]; *SPARC/ON* (secreted protein, acidic, cysteine-rich/osteonectin); *RUNX2* (runt-related transcription factor 2); *SPP1/OP* (secreted phosphoprotein 1/osteopontin); and *SP7/OSX* (Sp7 transcription factor/osterix).

3.4.1. Differences at 21% O_2 (Figure 3)

Adult BM-MSCs revealed, as expected, the highest basic expression level of typical osteogenic markers, such as *BSP*, *BMP2*, *BMP4*, *OP* and *OSX*, in comparison to neonatal normoxic USSCs or CB-MSCs^{ABCD}. Expression of *BMP4* and *OP* in neonatal cord blood subtypes was higher in CB-MSCs^{ABCD} in comparison with USSCs.

3.4.2. Differences at 3% O_2 (Figure 3)

At 3% oxygen tension *BMP2*, *BMP4*, *ON* and *OSX* were upregulated in USSCs and CB-MSCs compared to their normoxic counterparts. Interestingly, *BSP* and *OC* were downregulated in *HOX*-negative USSCs but upregulated in *HOX*-positive CB-MSCs^{ABCD} upon low oxygen tension, again suggesting a different kind of regulation

DOI: 10.1002/term

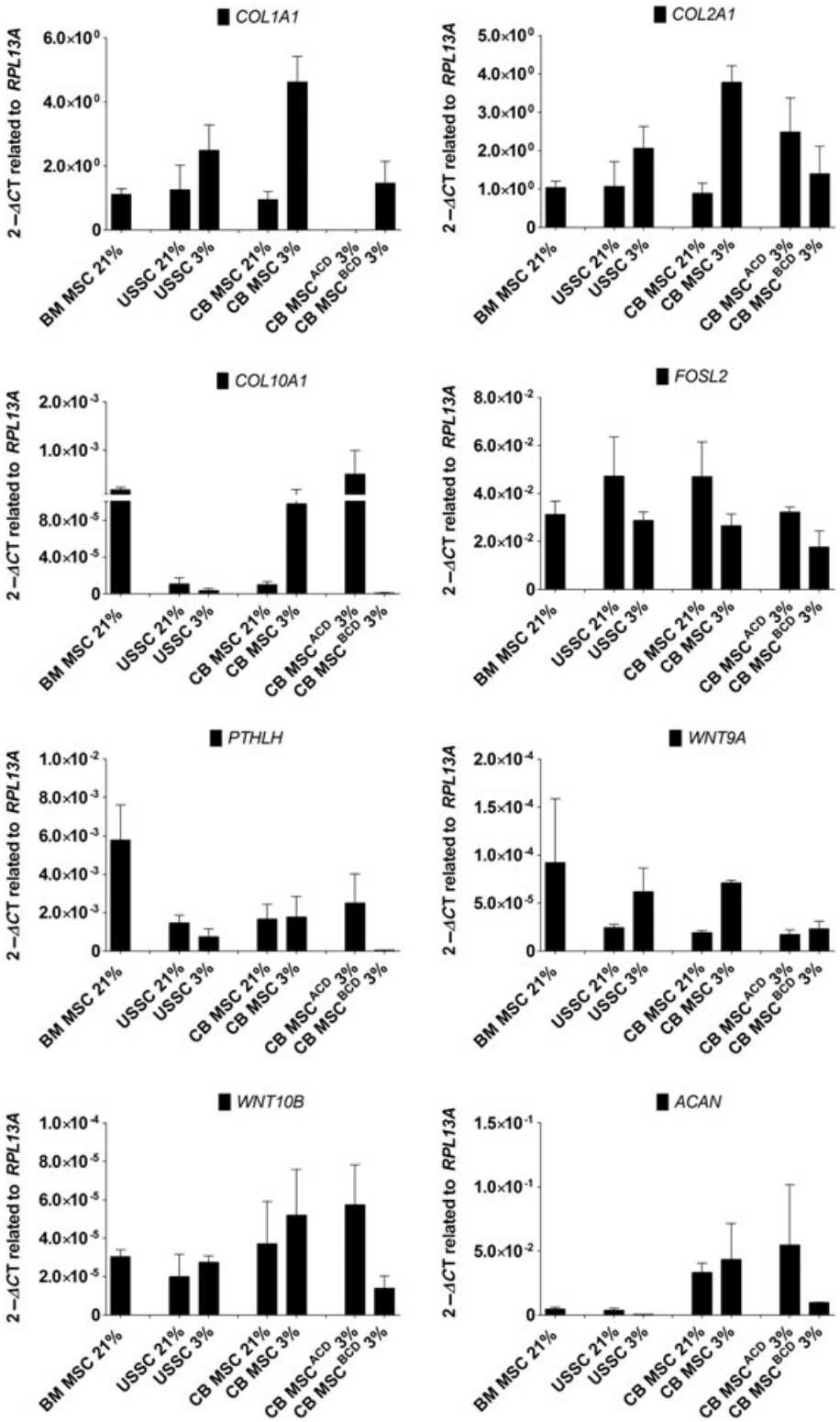

Figure 2. Expression of chondrogenesis-associated genes in adult and neonatal cord blood stromal cells at 21% vs 3% O_2. Cell subtypes were generated and cultivated at either 21% or 3% O_2; adult BM-MSCs were applied as the control population; data were normalized to the reference gene, *RPL13A*, applying the ΔC_T method; mean values are given as SE

between *HOX*-positive and *HOX*-negative subtypes. Discriminating factors between CB-MSCs^{BCD} and CB-MSCs^{ACD} seemed to be *BMP4* (highest in CB-MSCs^{BCD} subtype) and *RUNX2* (highest in CB-MSCs^{ACD} subtype), maybe due to the lack of *HOXA10*, which can positively regulate *RUNX2*, *OC* and *BSP* (Hassan *et al.*, 2007).

3.5. Definition of typical bone signatures in neonatal cord blood subtypes associated with the individual HOX code

In order to correlate the specific chondro-osteogenic signatures of neonatal cord blood subtypes with BM-MSCs,

DOI: 10.1002/term

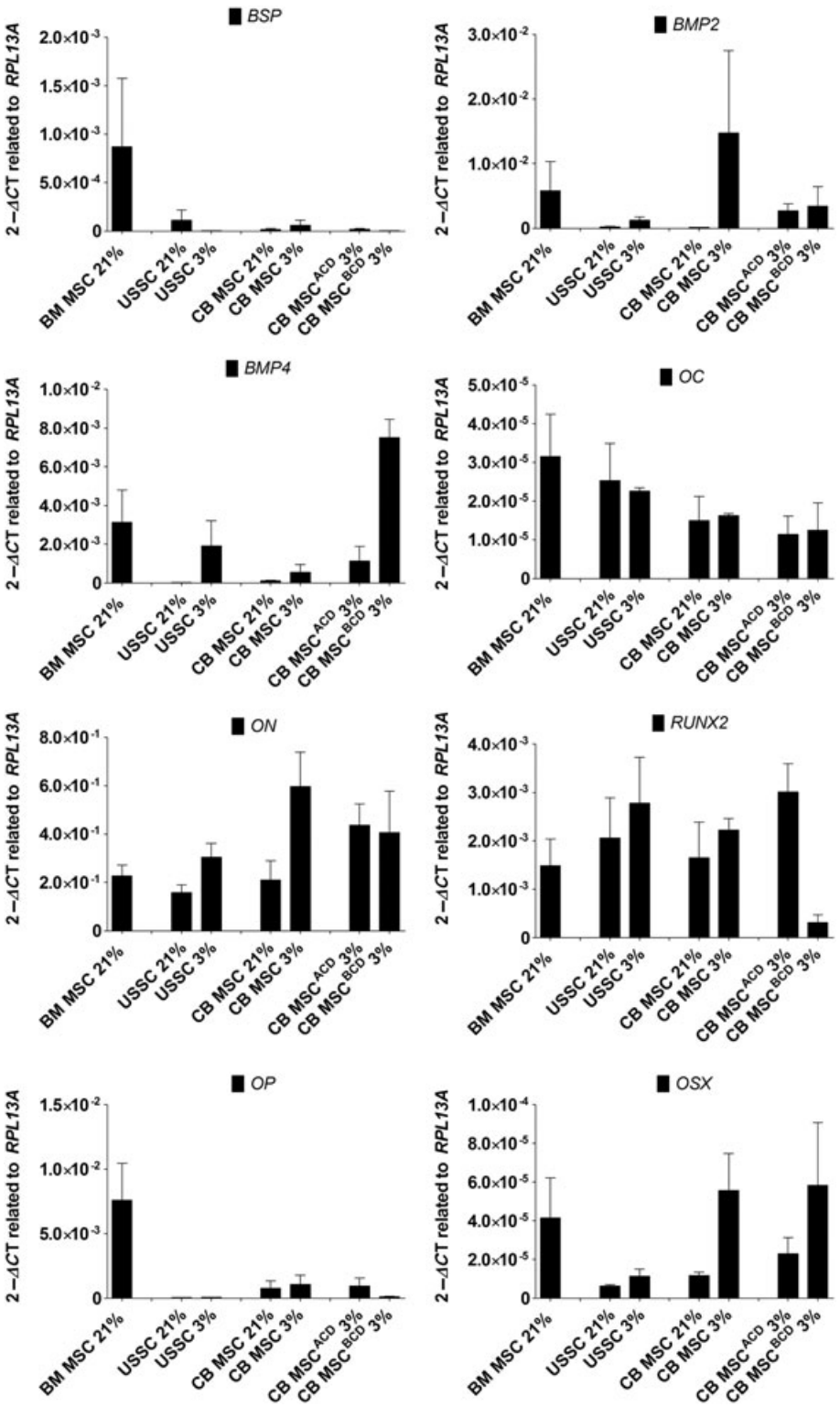

Figure 3. Expression of osteogenesis-associated genes in adult and neonatal cord blood stromal cells at 21% O_2 normoxia vs 3% O_2. Cell subtypes were generated and cultivated at either 21% or 3% O_2; adult BM-MSCs were applied as the control population; data were normalized to the reference gene, *RPL13A*, applying the ΔC_T method; mean values are given as SE

significant gene expression differences (positive fold change >4, negative fold change > −4) were determined (Figure 4). Table S2 (see supporting information) shows all fold change differences.

In comparison to BM-MSCs, significant differences were found for *ACAN*, strongly upregulated at normoxia (9.35) and at low oxygen tension (12.24) CB-MSCs^{ABCD} and 3% O_2 CB-MSCs^{ACD} (15.44). Interestingly, *ACAN* was uniquely downregulated in 3% O_2 USSCs (−22.48) vs normoxic USSCs. *COL1A1* and *COL2A2* were detected at comparable levels in normoxic USSCs and CB-MSCs^{ABCD}, but upregulated in subtypes at low oxygen tension, with the highest significant difference in 3% O_2 CB-MSCs (4.29). *COL10A1* was significantly downregulated in

DOI: 10.1002/term

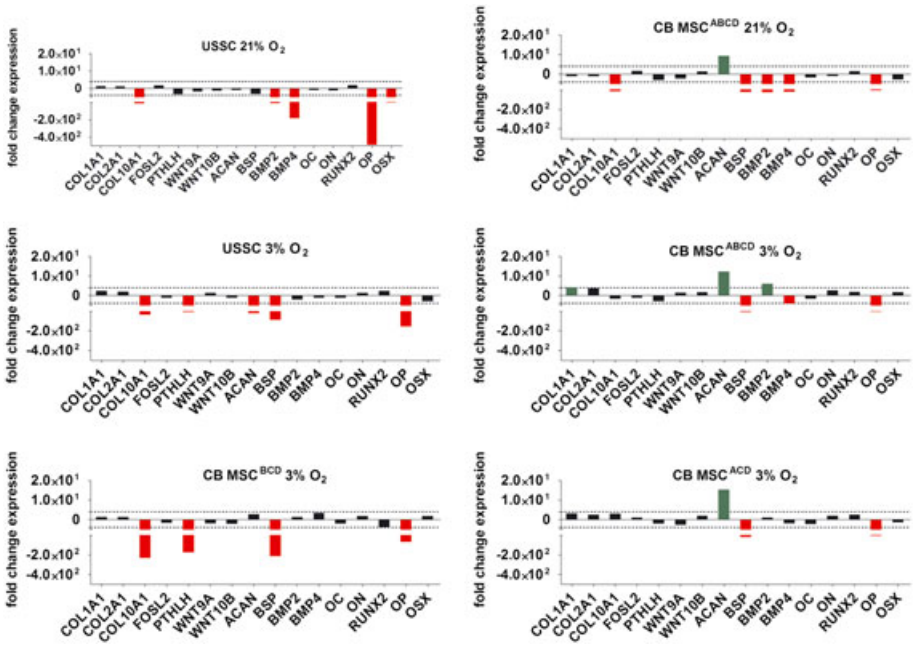

Figure 4. Specific chondro-osteogenic signatures of neonatal cord blood stromal subtypes at normoxia and low oxygen tension. Cell subtypes were generated and cultivated at either 21% or 3% O_2; adult BM-MSCs (n = 3) were applied as the control population and normalization was performed by applying the $\Delta\Delta C_T$ method; values are given as respective fold changes in comparison to BM-MSCs (n = 3), using the formula $2^{-\Delta\Delta C_T}$; negative fold changes of mean values were calculated by the negatives of their inverses; lines within graphs were set to 4 and −4, marking significant fold changes; green, significantly upregulated genes; red, significantly downregulated genes

normoxic USSCs (−16.02) and CB-MSCs^{ABCD} (−17.52), and in 3% O_2 USSCs (−37.59) and CB-MSCs^{BCD} (−231.35). The lowest expression of *PTHLH* was found in 3% O_2 CB-MSCs^{BCD} (−174.60) and, to a lesser extent, in 3% O_2 USSCs (−7.11). *BSP* expression varied in defined subtypes and showed the lowest expression in 3% O_2 CB-MSCs^{BCD} (−215.13). In addition, *BMP2* was upregulated in 3% O_2 CB-MSCs^{BCD} (6.01), but downregulated in normoxic USSCs (−12.07) and CB-MSCs^{ABCD} (−26.49), in accordance with *BMP4*, which was lowest in normoxic USSCs (−182.96) and CB-MSCs^{ABCD} (−21.76). Finally, the strongest overall downregulation was observed for *OP* in normoxic USSCs (−485.62), but was also significantly downregulated in all other subtypes tested.

3.6. Correlation of chondrogenic and osteogenic differentiation potentials with regard to distinct stromal cell subtypes

In order to compare the *in vitro* differentiation potentials of analysed stromal subtypes, chondrogenic and osteogenic differentiation were performed, and the resulting safranin-O and alizarin and von Kossa staining of all individual cell lines (each *HOX* subtype, n = 3) are presented in Figures S2 and S3 (see supporting information).

3.6.1. In vitro chondrogenesis

By safranin-O staining (Figure 5, right panel), the chondrogenic potential was determined in all tested subtypes except for CB-MSCs^{BCD}, since no proper pellet formation occurred repeatedly. Despite of the biological heterogeneity within individual subtypes (see supporting information, Figure S2), all cord blood-derived stromal cells revealed a superior deposition of proteoglycans in comparison with BM-MSCs. Measurements of pellet areas and diameters disclosed a decrease in pellet size of USSCs but an increase of pellet size in all CB-MSCs subtypes upon low oxygen tension (see supporting information, Figure S4).

3.6.2. In vitro osteogenesis

Normoxic USSCs revealed the highest *in vitro* differentiation capacity for osteogenesis, reflected by the visualized mineralization level of the cells (Figure 5). Weaker mineralization was found in normoxic CB-MSCs^{ABCD} and BM-MSCs (only one BM-MSCs line showed strong calcification comparable to normoxic USSCs). At 3% O_2, *HOX*-negative USSCs lines tested revealed strong calcification, similar to that of normoxic USSCs. For *HOX*-positive CB-MSCs^{ABCD} at 3% O_2, a higher calcification in comparison to normoxic CB-MSCs^{ABCD} was found in two of three cell lines, whereas one cell line was weakly stained. CB-MSCs^{ACD} at 3% O_2 consistently showed stronger calcification, compared to normoxic CB-MSCs^{ABCD}. Most interestingly, no calcification was detectable in the CB-MSCs^{BCD} subtype, as in three independent experiments the cells were repeatedly detached and lost during differentiation, supporting the qPCR results (Figure S2), since themineralization genes

DOI: 10.1002/term

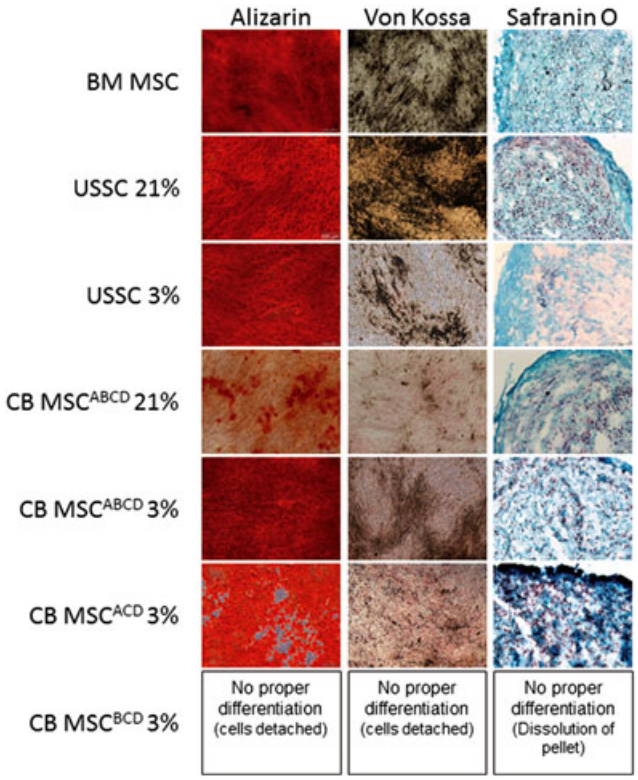

Figure 5. Representative staining disclosing chondro-osteogenic differentiation potential of distinct 3% O_2 subtypes compared to normoxic controls. Stromal subtypes were either cultured in osteogenic differentiation medium for 14 days and stained with alizarin and von Kossa or cultured in chondrogenic differentiation medium for 21 days and stained with safranin O (including a Fast Green counterstain). Micrographs were acquired at room temperature, using a standard Olympus CKX41 inverted microscope and a SIS-View FireWire camera fitted with a UPlanFLN ×10/0.3 Ph1 objective (alizarin and von Kossa) and a LUCPlan ×40/0.6 Ph2 objective (safranin O): pictures were taken using CellD software (Olympus Soft Imaging GmbH, v. 2.7, build 1224); single pictures (jpg format) were then imported into Microsoft Powerpoint 2010 and combined into a single composite image; the brightness and contrast of the images was adjusted, if necessary, using the picture tools function of Microsoft Powerpoint 2010

BSP, *OC* and *RUNX2* were detected at very low levels, maybe due to absent *HOXA10* expression (Hassan *et al.*, 2007).

3.6.3. In vivo bone formation assay

Since *in vitro* differentiation assays do not necessarily reflect the *in vivo* bone formation capacity, *in vivo* heterotopic bone formation was performed by applying an established assay (Sacchetti *et al.*, 2007). Exemplary results are presented in Figure 6. As expected, the population of adult BM-MSCs ($n = 2$) revealed consistent bone-formation capacity, confirming the *in vitro* data (Figure 5). In the cord blood-derived USSC subtype, two of four cell lines tested were positive for *in vivo* osteogenic differentiation and one of three CB-MSCs^{ABCD} lines developed bone. This is not completely in line with the *in vitro* data, since all USSCs and all CB-MSCs lines were consistently positively stained by alizarin and von Kossa *in vitro*. Regarding the biological heterogeneity of cell lines, possible factors responsible for proper bone formation in single lines have to be further elucidated. However, in comparison to cord blood-derived subtypes, cord-derived UC-MSCs ($n = 3$) never formed bone *in vivo*.

4. Discussion

As early as 1994, subpopulations of haematopoietic stem cells revealing unique features were defined by their specific *HOX* code (Sauvageau *et al.*, 1994). For stromal cell types this approach is likewise interesting with regard to regenerative approaches, as it is mandatory to know in detail the typical signatures linked to the differentiation capacities of applied cells, but also the molecular background of the site of injury (Leucht *et al.*, 2008). The results presented here clearly demonstrate a close interrelationship between oxygen tension, differentiation potential and the inherent *HOX* codes of stromal subtypes.

Interestingly, *HOX*-positive subtypes of clonally generated neonatal cord blood stromal cell lines were most abundant at 3% O_2 (Figure 1B). However, an upregulation of *HOX* genes upon low oxygen tension would be unexpected, as the *HOX*-associated microRNA mir-210 was found to be strongly upregulated by HIF1α, the most prominent hypoxia-inducible factor, and should therefore rather lead to a downregulation of *HOX* genes (Atashi *et al.*, 2015; Mathew and Simon, 2009; Palomaki *et al.*, 2013). Moreover a normoxic stabilization of *HIF1*α has already been described in neonatal stromal subtypes at ambient conditions by our group (Buchheiser *et al.*,

DOI: 10.1002/term

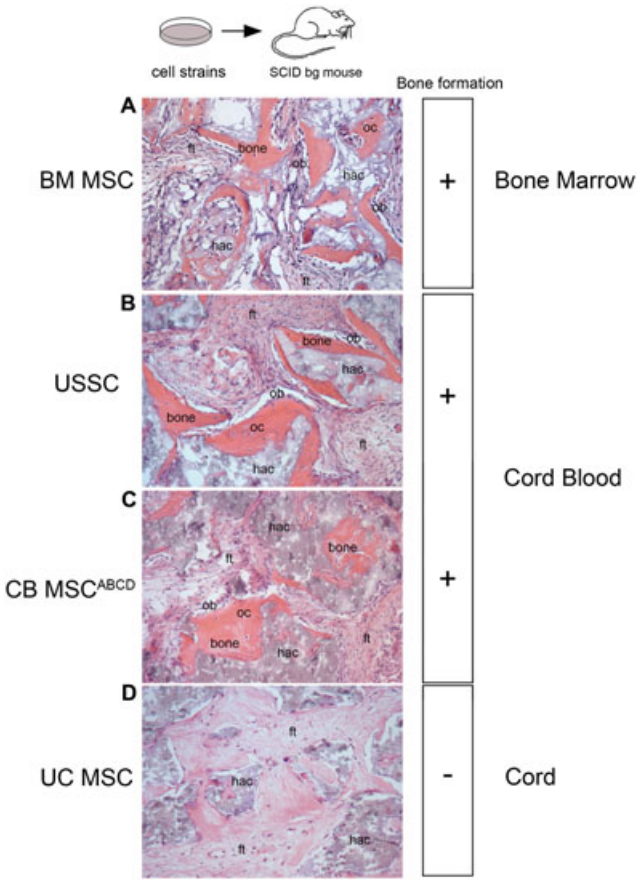

Figure 6. Development of heterotopic bone in transplants of distinct stromal cell subtypes: histology of human adult BM-MSCs, neonatal cord blood-derived USSCs, CB-MSCs and cord-derived UC-MSC transplants harvested 8 weeks post-transplantation; H&E staining. Abundant new delete fully bone was detected in BM-MSCs (A), cord blood-derived USSCs (B) and CB-MSCs (C), but never in cord-derived UC-MSCs (D). Bone contains differentiated osteoblasts (ob) and osteocytes (oc) (A–C); ft, fibroblastic tissue; hac, hydroxyapatite carrier

2012) and the HIF1α-dependent maintenance in an undifferentiated state was confirmed by others (Palomaki *et al.*, 2013; Park *et al.*, 2013). In addition, cultivation of the respective cell lines at 21% O_2 revealed no alteration of the inherent *HOX* code and no significant passage-dependent loss of expression was verified within clonal subtypes (Laitinen *et al.*, 2015). Maintenance of homeotic gene expression patterns requires a second set of factors, encoded by the polycomb (PcG) and trithorax (trxG) group genes, regulating the epigenetic maintenance of the *HOX* code by modifying the chromatin structure.

Mesenchymal condensation, encountering low oxygen tension as a prerequisite for proper cartilage formation, is the earliest event of chondrogenesis accompanied by expression of *HoxA* and *HoxD* cluster genes in vertebrates (Goldring *et al.*, 2006; Kmita *et al.*, 2005). *HoxA* and *HoxD* genes are involved in cartilage and bone formation and it has been proposed that their restricted spatial expression is controlled by a gradient of morphogens, like FGFs (Lewandoski *et al.*, 2000). As under normal *in vitro* culture conditions such a gradient is missing, the expression of *HOXA* and *HOXD* genes may be variable. One prominent *HOX* gene associated with cartilage and bone formation is *HOXA2*, which has been shown to antagonize bone formation during development (Kanzler *et al.*, 1998). Moreover, *HOXA10* activates *RUNX2* transcription, leading to osteoblastogenesis (Hassan *et al.*, 2007). By microarray gene expression profiling, many HOX proteins were defined as molecular targets of BMP-mediated gene transcription during early differentiation stages, linking the *HOX* expression patterns with bone formation (Balint *et al.*, 2003; Hassan *et al.*, 2006). *HOXA2* and *HOXA10* are consistently expressed in all *HOX*-positive subtypes presented here, but are absent in *HOX*-negative USSCs and the CB-MSCs^{BCD} subtype missing expression within the HOXA-cluster. Interestingly, for three of three normoxic USSCs and three of three USSCs at 3% O_2, strong mineralization was detected by alizarin and von Kossa staining (see supporting information, Figure S2) but HOXA-cluster negative CB-MSCs^{BCD} failed to differentiate properly into the chondro-osteogenic lineage. This supposes a different kind of regulation between single subtypes, and *HOXA2* and *HOXA10* expression seems not to be mandatory in USSCs for proper chondro-osteogenic differentiation, but to be relevant in the CB-MSCs^{BCD} subtype. In addition, the paralogous *HOXC10* gene is completely absent in CB-MSCs^{BCD}, explaining the loss of chondro-osteogenic potential (Hostikka *et al.*, 2009). Other examples of subtype-specific gene regulation were found for *COL10A1*, *ACAN* and *BSP*, all downregulated in *HOX*-negative USSCs at 3% O_2 but upregulated in *HOX*-positive CB-MSCs^{ABCD}. Furthermore, co-culture of *HOX*-negative USSCs with *HOX*-positive CB-MSCs leads to an upregulation of *HOX* genes in USSCs, in line with an upregulation of *ACAN* and downregulation of *BSP* (Liedtke *et al.*, 2013), again supporting that the HOX code of a cell is closely linked to the differentiation potentials of individual subtypes. A major function of ACAN is to resist compression in cartilage, which is supported by the qPCR data in combination with the chondropellet sizes analysed here. Expression of the later chondrogenic marker *COL10A1* was highest in CB-MSCs^{ACD} subtype, maybe due to activation of *COL10A1* by *RUNX2* (Gu *et al.*, 2014; Li *et al.*, 2011; Zheng *et al.*, 2003).

Besides the complex regulation of chondro-osteogenic marker genes in the *HOX* expression background of a cell, strong inherent cell heterogeneity, on a bulk and not clonal level, may lead to misinterpretation of data (Kluth *et al.*, 2012; McKenna *et al.*, 2015; Viswanathan *et al.*, 2015). Here, clonally derived cell lines were applied and subtypes defined by specific *HOX* codes. The subtype-specific *HOX* codes revealed in this study were most likely established early in embryogenesis and maintained epigenetically through the modification of chromatin by the polycomb and trithorax group genes (Francis and Kingston, 2001). A putative circulation of the neonatal cord blood CB-MSCs^{ABCD} subtype through the bone marrow niche might be feasible, since BM-MSCs reveal a nearly similar *HOX* code. Possibly, *HOX*-negative USSCs have not yet migrated through the periphery and have therefore kept a negative fetal

DOI: 10.1002/term

liver-associated *HOX* code. The higher abundance of CB-MSCs clones at 3% O_2 presented here could be explained by the hypoxic conditions within the bone marrow niche, leading hypothetically to the preference of clones. However, our data present a stable *HOX* code after generation of cell lines in close relation to the endochondral signature of neonatal cord blood subtypes, in line with the inherent differentiation potential. Reinisch *et al*. (2015) described the underlying differences in epigenetic programmes comparing BM-MSC, white adipose tissue-, umbilical cord- (not cord blood) and skin-derived MSC endochondral signatures. These findings strongly suggest a similar epigenetic diversity in neonatal cord blood-derived stromal cell subtypes defined here.

However, regarding the limitations of the study here to be improved in future, research should be further focused on the correlation of endochondral signatures to more extensive *in vivo* data, since *in vitro* data might not be sufficient and do not necessarily signify the *in vivo* bone formation capacity of different cell sources at a clonal level (Bianco *et al.*, 2010; Bonewald *et al.*, 2003).

5. Conclusion

The results presented here underline the necessity to comprehensively characterize possible cell sources supposed for regeneration of cartilage and bone, due to strong heterogeneity. Prior to any differentiation assay, distinct subtypes could already be defined here by the stable expression of specific *HOX* codes at normoxia and low oxygen tension. Furthermore, characteristic chondro-osteogenic bone signatures were determined for each subgroup, manifesting a distinct kind of gene regulation, mainly between *HOX*-negative USSCs and *HOX*-positive CB-MSCs. This approach might enhance the possibility of prospectively finding the most adequate cell source and offer the perspective to match the given cell population to the topographic site of injury.

Acknowledgments

We would like to thank the Deutscher Akademischer Austauschdienst (DAAD) for supporting this project (University Dialogue with South Europe; Grant No. DAAD-ID 57139466). We are very grateful to Professor Paolo Bianco (Sapienza University, Rome, Italy) for his essential impact in creating and discussing the *in vivo* data. In addition we would like to thank Daniela Stapelkamp for her excellent technical support.

Conflict of interest

The authors declare no conflicts of interest.

Author contributions

St.L., conception and design, collection and/or assembly of data, PCR data analysis and interpretation and manuscript writing; B.S., collection and/or assembly of *in vivo* data, histology and data analysis; A.L., collection and/or assembly of data for low oxygen cell lines and data analysis; S.D., collection and/or assembly of *in vivo* data, histology and data analysis; R.K., collection and/or assembly of *in vitro* differentiation data and data analysis; Sa.L., provision of additional cell lines and critical reading of manuscript; M.R., conception and design of *in vivo* data, histology and critical reading of manuscript; and G.K., conception and design and final approval of manuscript.

References

Ackema KB, Charite J. 2008; Mesenchymal stem cells from different organs are characterized by distinct topographic *Hox* codes. *Stem Cells Dev* **17**: 979–991.

Atashi F, Modarressi A, Pepper MS. 2015; The role of reactive oxygen species in mesenchymal stem cell adipogenic and osteogenic differentiation: a review. *Stem Cells Dev* **24**(10): 1150–1163.

Balint E, Lapointe D, Drissi H, *et al.* 2003; Phenotype discovery by gene expression profiling: mapping of biological processes linked to BMP-2-mediated osteoblast differentiation. *J Cell Biochem* **89**: 401–426.

Bianco P, Robey PG, Saggio I, *et al.* 2010; 'Mesenchymal' stem cells in human bone marrow (skeletal stem cells): a critical discussion of their nature, identity, and significance in incurable skeletal disease. *Hum Gene Ther* **21**: 1057–1066.

Bianco P, Robey PG, Simmons PJ. 2008; Mesenchymal stem cells: revisiting history, concepts, and assays. *Cell Stem Cell* **2**: 313–319.

Bonewald LF, Harris SE, Rosser J, *et al.* 2003; von Kossa staining alone is not sufficient to confirm that mineralization *in vitro* represents bone formation. *Calcif Tissue Int.* **72**: 537–547.

Bosch J, Houben AP, Hennicke T, *et al.* 2013; Comparing the gene expression profile of stromal cells from human cord blood and bone marrow: lack of the typical 'bone' signature in cord blood cells. *Stem Cells Int* **2013**: 631984.

Bosch J, Houben AP, Radke TF, *et al.* 2012; Distinct differentiation potential of 'MSC' derived from cord blood and umbilical cord: are cord-derived cells true mesenchymal stromal cells? *Stem Cells Dev* **21**: 1977–1988.

Buchheiser A, Houben AP, Bosch J, *et al.* 2012; Oxygen tension modifies the 'stemness' of human cord blood-derived stem cells. *Cytotherapy* **14**(8): 967–982.

Busser H, Najar M, Raicevic G, *et al.* 2015; Isolation and Characterization of Human Mesenchymal Stromal Cell Subpopulations: Comparison of Bone Marrow and Adipose Tissue. *Stem Cells Dev* **24**(18): 2142–2457.

Chang HY, Chi JT, Dudoit S, *et al.* 2002; Diversity, topographic differentiation, and positional memory in human fibroblasts. *Proc Natl Acad Sci U S A* **99**: 12877–12882.

Francis NJ, Kingston RE. 2001; Mechanisms of transcriptional memory. *Nat Rev Mol Cell Biol* **2**: 409–421.

Goldring MB, Tsuchimochi K, Ijiri K. 2006; The control of chondrogenesis. *J Cell Biochem* **97**: 33–44.

Gu J, Lu Y, Li F, *et al.* 2014; Identification and characterization of the novel Col10a1 regulatory mechanism during chondrocyte hypertrophic differentiation. *Cell Death Dis* **5**: e1469.

Handschel J, Naujoks C, Langenbach F, *et al.* 2010; Comparison of ectopic bone formation of embryonic stem cells and cord blood stem cells *in vivo*. *Tissue Eng A* **16**: 2475–2483.

Harrington J, Sloan AJ, Waddington RJ. 2014; Quantification of clonal heterogeneity of mesenchymal progenitor cells in

dental pulp and bone marrow. *Connect Tissue Res* **55**(suppl 1): 62–67.
Hassan MQ, Tare R, Lee SH, *et al.* 2007; HOXA10 controls osteoblastogenesis by directly activating bone regulatory and phenotypic genes. *Mol Cell Biol* **27**: 3337–3352.
Hassan MQ, Tare RS, Lee SH, *et al.* 2006; BMP2 commitment to the osteogenic lineage involves activation of Runx2 by DLX3 and a homeodomain transcriptional network. *J Biol Chem* **281**: 40515–40526.
Hostikka SL, Gong J, Carpenter EM. 2009; Axial and appendicular skeletal transformations, ligament alterations, and motor neuron loss in *Hoxc10* mutants. *Int J Biol Sci* **5**: 397–410.
Izpisua-Belmonte JC, Duboule D. 1992; Homeobox genes and pattern formation in the vertebrate limb. *Dev Biol* **152**: 26–36.
Kaltz N, Funari A, Hippauf S, *et al.* 2008; *In vivo* osteoprogenitor potency of human stromal cells from different tissues does not correlate with expression of POU5F1 or its pseudogenes. *Stem Cells* **26**: 2419–2424.
Kanzler B, Kuschert SJ, Liu YH, *et al.* 1998; Hoxa-2 restricts the chondrogenic domain and inhibits bone formation during development of the branchial area. *Development* **125**: 2587–2597.
Karsenty G. 2008; Transcriptional control of skeletogenesis. *Annu Rev Genom Hum Genet* **9**: 183–196.
Klontzas ME, Kenanidis EI, Heliotis M, *et al.* 2015; Bone and cartilage regeneration with the use of umbilical cord mesenchymal stem cells. *Expert Opin Biol Ther* **15**: 1541–1552. ISSN:1471–2598.
Kluth SM, Buchheiser A, Houben AP, *et al.* 2010; DLK-1 as a marker to distinguish unrestricted somatic stem cells and mesenchymal stromal cells in cord blood. *Stem Cells Dev* **19**: 1471–1483.
Kluth SM, Radke TF, Kogler G. 2012; Potential application of cord blood-derived stromal cells in cellular therapy and regenerative medicine. *J Blood Transfus* **2012**: 365182.
Kmita M, Tarchini B, Zakany J, *et al.* 2005; Early developmental arrest of mammalian limbs lacking *HoxA/HoxD* gene function. *Nature* **435**: 1113–1116.
Kogler G, Sensken S, Airey JA, *et al.* 2004; A new human somatic stem cell from placental cord blood with intrinsic pluripotent differentiation potential. *J Exp Med.***200**: 123–135.
Krebsbach PH, Kuznetsov SA, Satomura K, *et al*. 1997; Bone formation in vivo: comparison of osteogenesis by transplanted mouse and human marrow stromal fibroblasts. *Transplantation* **63**(8): 1059–1069.
Krumlauf R. 1994; *Hox* genes in vertebrate development. *Cell* **78**: 191–201.
Laitinen A, Lampinen M, Liedtke S, *et al.* 2015; The effects of culture conditions on the generation and functionality of the mesenchymal stromal cells from cord blood. *Cytotherapy* **2016**: 423–437.
Laitinen A, Nystedt J, Laitinen S. 2011; The isolation and culture of human cord blood-derived mesenchymal stem cells under low oxygen conditions. *Methods Mol Biol* **698**: 63–73. DOI: 10.1007/978-1-60761-999-4_6.
Langenbach F, Berr K, Naujoks C, *et al.* 2011; Generation and differentiation of microtissues from multipotent precursor cells for use in tissue engineering. *Nat Protoc* **6**: 1726–1735.
Leucht P, Kim JB, Amasha R, *et al.* 2008; Embryonic origin and Hox status determine progenitor cell fate during adult bone regeneration. *Development* **135**: 2845–2854.
Lewandoski M, Sun X, Martin GR. 2000; Fgf8 signalling from the AER is essential for normal limb development. *Nat Genet* **26**: 460–463.
Li F, Lu Y, Ding M, *et al.* 2011; Runx2 contributes to murine *Col10a1* gene regulation through direct interaction with its *cis*-enhancer. *J Bone Miner Res* **26**: 2899–2910.
Liedtke S, Buchheiser A, Bosch J, *et al.* 2010; The *HOX* code as a 'biological fingerprint' to distinguish functionally distinct stem cell populations derived from cord blood. *Stem Cell Res* **5**: 40–50.
Liedtke S, Freytag EM, Bosch J, *et al.* 2013; Neonatal mesenchymal-like cells adapt to surrounding cells. *Stem Cell Res* **11**: 634–646.
Mathew LK, Simon MC. 2009; mir-210: a sensor for hypoxic stress during tumorigenesis. *Mol Cell* **35**: 737–738.
McKenna D, Matthay MA, Pati S. 2015; Correspondence to: Soliciting strategies for developing cell-based reference materials to advance mesenchymal stem/stromal cell research and clinical translation. *Stem Cells Dev* **23**: 1717–1718.
Palomaki S, Pietila M, Laitinen S, *et al.* 2013; HIF-1α is upregulated in human mesenchymal stem cells. *Stem Cells* **31**: 1902–1909.
Park IH, Kim KH, Choi HK, *et al.* 2013; Constitutive stabilization of hypoxia-inducible factor-α selectively promotes the self-renewal of mesenchymal progenitors and maintains mesenchymal stromal cells in an undifferentiated state. *Exp Mol Med* **45**: e44.
Reinisch A, Etchart N, Thomas D, *et al.* 2015; Epigenetic and *in vivo* comparison of diverse MSC sources reveals an endochondral signature for human hematopoietic niche formation. *Blood* **125**: 249–260.
Sacchetti B, Funari A, Michienzi S, *et al.* 2007; Self-renewing osteoprogenitors in bone marrow sinusoids can organize a hematopoietic microenvironment. *Cell* **131**: 324–336.
Sauvageau G, Lansdorp PM, Eaves CJ, *et al.* 1994; Differential expression of homeobox genes in functionally distinct $CD34^+$ subpopulations of human bone marrow cells. *Proc Natl Acad Sci U S A* **91**: 12223–12227.
Schmittgen TD, Livak KJ. 2008; Analyzing real-time PCR data by the comparative C_T method. *Nat Protoc* **3**: 1101–1108.
Viswanathan S, Keating A, Deans R, *et al.* 2015; Soliciting strategies for developing cell-based reference materials to advance mesenchymal stromal cell research and clinical translation. *Stem Cells Dev* **23**: 1157–1167.
Wegmeyer H, Broske AM, Leddin M, *et al.* 2013; Mesenchymal stromal cell characteristics vary depending on their origin. *Stem Cells Dev* **22**: 2606–2618.
Zheng Q, Zhou G, Morello R, *et al.* 2003; Type X collagen gene regulation by Runx2 contributes directly to its hypertrophic chondrocyte-specific expression *in vivo*. *J Cell Biol* **162**: 833–842.

Supporting information on the internet

The following supporting information may be found in the online version of this article:

Figure S1. HOX codes of individual cell subtypes under normoxia and low oxygen tension
Figure S2. Chondrogenic differentiation capacity of stromal cell subtypes under normoxia and low oxygen tension
Figure S3. Osteogenic differentiation capacity of stromal cell subtypes under normoxia and low oxygen tension
Figure S4. Chondrogenic differentiation potential of neonatal stromal cell subtypes under normoxia (21% O_2) and low oxygen tension (3% O_2) in comparison with adult BM-MSCs
Table S1. *RPL13A* was used as reference gene in qPCR experiments
Table S2. *GAPDH* was used as reference gene in RT–PCR experiments
Table S3. Fold change differences

Supplemental data

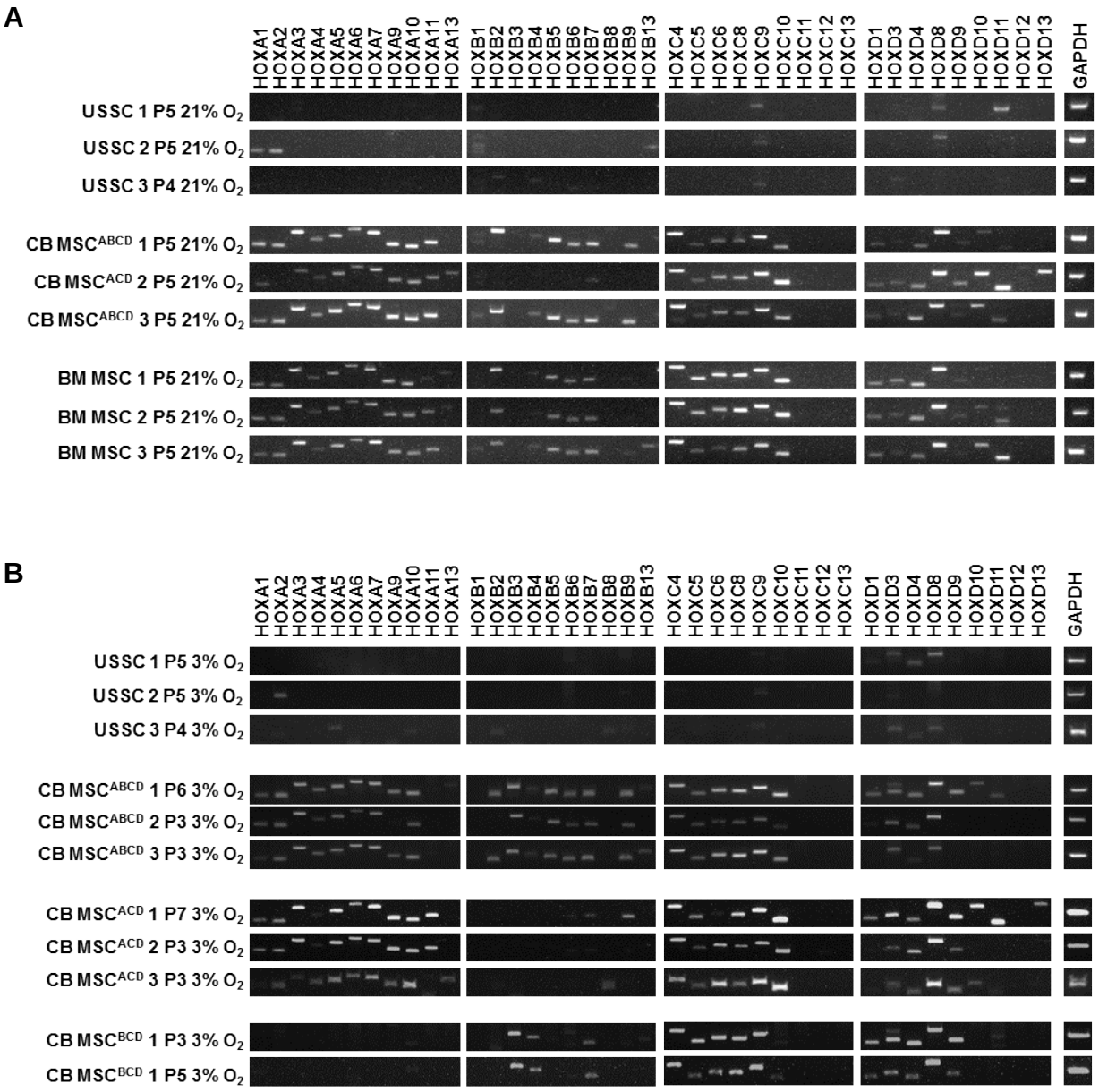

Supplemental fig. 1: HOX codes of individual cell subtypes under normoxia and low oxygen tension. a Stromal cells were generated and cultivated at 21% O_2. **b** Stromal cells were generated and cultivated at 3% O_2. Individual *HOX* gene expression patterns were determined by conventional RT-PCR applying 50ng cDNA with *GAPDH* as reference gene. DNA fragments were separated by electrophoresis on a 2% agarose/TBE gel and visualized by Midori Green. P: passage; USSC: unrestricted somatic stromal cell; CB MSC: cord blood multipotent stromal cell; BM MSC: bone marrow mesenchymal stromal cell; TBE: Tris/boric acid/EDTA.

HOX codes of individual cell subtypes under normoxia and low oxygen tension:

USSC are devoid from *HOX* gene expression or reveal rather marginal expression in only single *HOX* genes and are therefore regarded as *HOX*-negative (HOX^-) cell type. CB MSC are defined by their typical expression pattern of several *HOX* genes in all four clusters (CB MSC^{ABCD}) or in cluster A, C and D (CB MSC^{ACD}) or in cluster B, C and D (CB MSC^{BCD}). Variations in single *HOX* genes are due to biological heterogeneity of clonal populations. Adult BM MSC and neonatal CB MSC^{ABCD} share high similarities in their *HOX* expression pattern.

Primer sequences of genes associated with chondro-osteogenesis

Primer	Sequence 5´- 3´	length [bp]	product size [bp]
COL1A1_for	CCCTCCCCAGCCACAAAGAGT	21	246
COL1A1_rev	CACCTTGCCGTTGTCGCAGAC	21	
COL2A1_for	AGGATGTCCAGGAGGCTGGC	20	212
COL2A1_rev	GGCAGTGGCGAGGTCAGTTG	20	
COL10A1_for	ACGCTGAACGATACCAAATG	20	117
COL10A1_rev	CTTGCTCTCCTCTTACTGCT	20	
FOSL2_for	GGCTCAGGCAGTGCATTCAT	20	258
FOSL2_rev	ACGCTTCTCCTCCTCTTCAGG	21	
PTHLH_for	GTGTTCCTGCTGAGCTACGC	20	173
PTHLH_rev	GCTGTGTGGATTTCTGCGATCA	22	
WNT9A_for	TCAAGCAAGGATCTGCGAGC	20	166
WNT9A_rev	GCTTGCCCACCTCATGGAAA	20	
WNT10B_for	TGAGCTCGGTGAGAGCAAAG	20	204
WNT10B_rev	TTAAACCGTGGGGAGACTGC	20	
ACAN_for	ACTGTTACCGCCACTTCCC	19	130
ACAN_rev	TCTTGGGCATTGTTGTTGAC	20	
IBSP/BSP_for	GGGCAGTAGTGACTCATCCG	20	214
IBSP/BSP_rev	AAGCTGGATTGCAGATAACCC	21	
BMP2_for	CGCTCTTTCAATGGACGTGT	20	98
BMP2_rev	CAACGCTAGAAGACAGCGGG	20	
BMP4_for	CCACCACGAAGAACATCTGG	20	96
BMP4_rev	ACGTCGTTCTCAGGGATGC	19	
BGLAP/OC_for	CCTCACACTCCTCGCCCTATT	21	117
BGLAP/OC_rev	CCCTCCTGCTTGGACACAAA	20	
SPARC/ON_for	TAAACCCCTCCACATTCCCGCG	22	159
SPARC/ON_rev	TTCTTGCTGAGGGGCTGCCAAG	22	
RUNX2_for	GAGTGGACGAGGCAAGAG	18	215
RUNX2_rev	GGACACCTACTCTCATACTG	20	
SPP1/OP_for	GCCGAGGTGATAGTGTGGTT	20	149
SPP1/OP_rev	AACGGGGATGGCCTTGTATG	20	
SP7/OSX_for	TGCTTGAGGAGGAAGTTCAC	20	153
SP7/OSX_rev	CTGAAAGGTCACTGCCCAC	19	
RPL13A_for	GAGGTATGCTGCCCCACAAA	20	136
RPL13A_rev	TTCAGACGCACGACCTTGAG	20	

Supplemental table 1: *RPL13A* was used as reference gene in qPCR experiments. If applicable, common synonyms appear behind official gene symbols separated by a slash.

Primer sequences of *HOX* genes

Primer	Sequence 5´- 3´	length [bp]	product size [bp]
HOXA1_for	ATCGGAGACATCTTCTCCA	19	178bp
HOXA1_rev	CAGGTACTTGTTGAAGTGG	19	
HOXA2_for	TCAGCCACAAAGAATCCCT	19	175bp
HOXA2_rev	CTCTCAGTCAAATCCAGCA	19	
HOXA3_for	TCAGAATGCCAGCAACAAC	19	310bp
HOXA3_rev	AGTGAGGTTCAGCAGATTG	19	
HOXA4_for	TGGATGAAGAAGATCCATG	19	233bp
HOXA4_rev	TGGTCTTTCTTCCACTTCA	19	
HOXA5_for	TAAGTCATGACAACATAGGC	20	276bp
HOXA5_rev	TTAAACGCTCAGATACTCAG	20	
HOXA6_for	ACTACCTGCACTTTTCTCC	19	359bp
HOXA6_rev	CGTGGAATTGATGAGCTTG	19	
HOXA7_for	TCCTACGACCAAAACATCC	19	324bp
HOXA7_rev	GTCCTTATGCTCTTTCTTCC	20	
HOXA9_for	AATGCTGAGAATGAGAGCGG	20	208bp
HOXA9_rev	TCTCGGTGAGGTTGAGCAG	19	
HOXA10_for	GATTCCCTGGGCAATTCC	18	191bp
HOXA10_rev	ACTTGTCTGTCCGTGAGG	18	
HOXA11_for	AACTTCAAGTTCGGACAGC	19	230bp
HOXA11_rev	AGACGCTGAAGAAGAACTC	19	
HOXA13_for	TACCTGGATATGCCAGTG	18	279bp
HOXA13_rev	GTATTCCCGTTCAAGTTC	18	
HOXB1_for	CAAGACAGCGAAGGTGTCA	19	208bp
HOXB1_rev	CTTCTGCTTCATTCGTCGG	19	
HOXB2_for	GTTCCCTTGGATGAAAGAG	19	271bp
HOXB2_rev	TTCGGTGAGGTCCAGCAA	18	
HOXB3_for	CAAATCTCCTTGGACCGGCTGTTG	24	282bp
HOXB3_rev	GTTCCAAGCGGCTGACCTTAG	21	
HOXB4_for	GCAAAGTTCACGTGAGCA	18	238bp
HOXB4_rev	TTGGGCAACTTGTGGTCT	18	
HOXB5_for	ATCAGCCATGATATGACCG	19	207bp
HOXB5_rev	GTTGTCCTTCTTCCACTTC	19	
HOXB6_for	GAATTCGTGCAACAGTTCC	19	175bp
HOXB6_rev	TATCTTGATCTGCCTCTCC	19	
HOXB7_for	GAGTAACTTCCGGATCTACC	20	182bp
HOXB7_rev	TGATCTGTCTTTCCGTGAGG	20	
HOXB8_for	TACGCAGACTGCAAGCTTG	19	324bp
HOXB8_rev	TTTGCTGCTGGGGAACTTG	19	
HOXB9_for	TGCTGTCTAATCAAAGACC	19	175bp
HOXB9_rev	AGAAACTCCTTCTCTAGCT	19	
HOXB13_for	AGCATTTGCAGACTCCAGC	19	251bp
HOXB13_rev	TGTTCTTCACCTTGGCGAG	19	

Primer	Sequence 5´- 3´	length [bp]	product size [bp]
HOXC4_for	AATTCACGTTAGCACGGTG	19	317bp
HOXC4_rev	AGTGGTCTTCAGAAGTACC	19	
HOXC5_for	TGACCAAACTGCACATGAG	19	205bp
HOXC5_rev	TTCTTCCACTTCATCCTGC	19	
HOXC6_for	ATGCAGCGAATGAATTCGC	19	239bp
HOXC6_rev	GTGGATGTGAGATTAGATTC	20	
HOXC8_for	CCAACACTAACAGTAGCGA	19	233bp
HOXC8_rev	GATCTTCACTTGTCTCTCG	19	
HOXC9_for	AAGCACAAAGAGGAGAAGG	19	281bp
HOXC9_rev	GTTTAGGACTGCTCCTTGT	19	
HOXC10_for	AGACACCTCGGATAACGAAG	20	190bp
HOXC10_rev	AATGGTCTTGCTAATCTCCAG	21	
HOXC11_for	TTTCTTCGACAACGCCTAC	19	360bp
HOXC11_rev	TCCGTCAGGTTCAGCATC	1	
HOXC12_for	AATCCGACTCCAGTTCGTC	19	184bp
HOXC12_rev	TCTGCCAGTTGCAACTTCG	19	
HOXC13_for	TGTACTGCTCCAAGGAGCA	19	152bp
HOXC13_rev	CTTCTCTAGCTCCTTCAGC	19	
HOXD1_for	TCTAAGAAAGGCAAACTCGC	20	170bp
HOXD1_rev	GTGTCATTCAGGTGCAAGC	19	
HOXD3_for	AGCAGAAGAACAGCTGTGC	19	187bp
HOXD3_rev	GTGAGATTCAGCAGGTTGG	19	
HOXD4_for	ATGAAGAAGGTGCACGTGA	19	160bp
HOXD4_rev	TGTGAGCGATTTCAATCCG	19	
HOXD8_for	TGAGACCACAAGCAGCTCC	19	284bp
HOXD8_rev	GTCTTCCTCCAGCTCTTGG	19	
HOXD9_for	CAACTTGACCCAAACAACC	19	182bp
HOXD9_rev	ACCTGTCTCTCTGTTAGGT	19	
HOXD10_for	CAAGAGTACAATAATAGCCC	20	278bp
HOXD10_rev	GGTGTATCAGACTTGATTTC	20	
HOXD11_for	AAGAGCAGCAGCGCAGTTGC	20	144bp
HOXD11_rev	AGGTTGAGCATCCGAGAGAG	20	
HOXD12_for	AACTTGAACATGACAGTGC	19	202bp
HOXD12_rev	TATTGGACAATTCCTTGCG	19	
HOXD13_for	ATATCGACATGGTGTCCAC	19	302bp
HOXD13_rev	CCGCTTGTCCTTGTTAATG	19	
GAPDH_for	GAGTCAACGGATTTGGTCGT	20	238bp
GAPDH_rev	TTGATTTTGGAGGGATCTCG	20	

Supplemental table 2: *GAPDH* was used as reference gene in RT-PCR experiments.

Fold change differences of chondro-osteogenic genes in BM MSC versus neonatal stromal cell types

Gene	USSC	CB MSC^{ABCD}	USSC	CB MSC^{ACD}	CB MSC^{BCD}	CB MSC^{ABCD}
COL1A1	1.16	-1.14	2.31	3.08	1.35	4.29
COL2A1	1.06	-1.14	2.05	2.46	1.39	3.76
COL10A1	-16.02	-17.52	-37.59	2.99	-231.35	-1.73
FOSL2	1.56	1.55	-1.05	1.06	-1.72	-1.14
PTHLH	-3.53	-3.14	-7.11	-2.09	-174.60	-2.92
WNT9A	-1.87	-2.37	1.36	-2.67	-1.96	1.57
WNT10B	-1.51	1.24	-1.09	1.92	-2.18	1.74
ACAN	-1.02	9.35	-22.48	15.44	2.70	12.24
BSP	-3.40	-25.68	-89.46	-20.51	-215.13	-6.50
BMP2	-12.07	-26.49	-1.98	1.11	1.38	6.01
BMP4	-182.96	-21.76	-1.15	-1.96	3.41	-4.10
OC	-1.04	-1.77	-1.17	-2.31	-2.11	-1.63
ON	-1.38	-1.05	1.39	1.99	1.86	2.72
RUNX2	1.73	1.39	2.34	2.54	-3.82	1.88
OP	-485.62	-8.81	-155.36	-7.10	-70.75	-6.37
OSX	-5.24	-2.82	-2.91	-1.42	1.78	1.70
	21% O_2		3% O_2			

Supplemental table 3: Fold change differences were calculated by the $2^{-\Delta\Delta Ct}$ method with BM MSC (n=3) as calibrator and *RPL13A* as reference gene. Negative fold changes of mean values were calculated by the negative of its inverse. Genes upregulated (green) or downregulated (red) in comparison with BM MSC revealed a significant fold change of >4 or <-4, respectively.

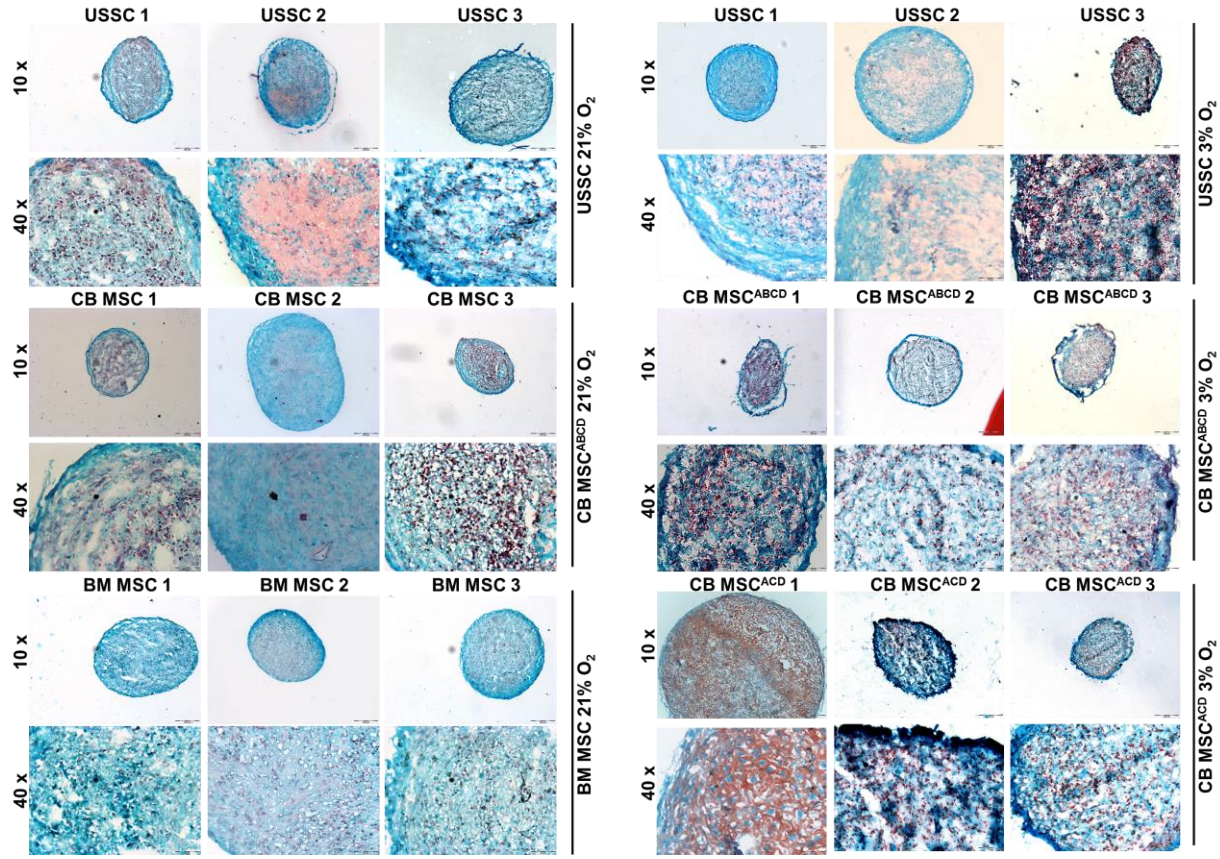

Supplemental fig. 2: Chondrogenic differentiation capacity of stromal cell subtypes under normoxia and low oxygen tension. a Normoxic samples **b** Hypoxic samples. Cells were differentiated in a pellet culture system into the chondrogenic lineage until day 21 and stained with Safranin O/Fast Green according to standard protocols. Micrographs were acquired at room temperature with a standard Olympus CKX41 inverted microscope fitted with UPlanFLN 10x/0.3 Ph1 objective and LUCPlan 40x/0.6 Ph2 objective and a SIS-View FireWire camera. Pictures were taken with Cell^{D} software (Olympus Soft Imaging GmbH, Version 2.7 (Build 1224)). Single pictures (jpg. format) were then imported into Microsoft Powerpoint 2010 and combined into a single composite image. Brightness and contrast of pictures was adjusted (if needed) with the picture tools function of Microsoft Powerpoint 2010. Scale bars: 200µm 10x objective and 50µm 40x objective.

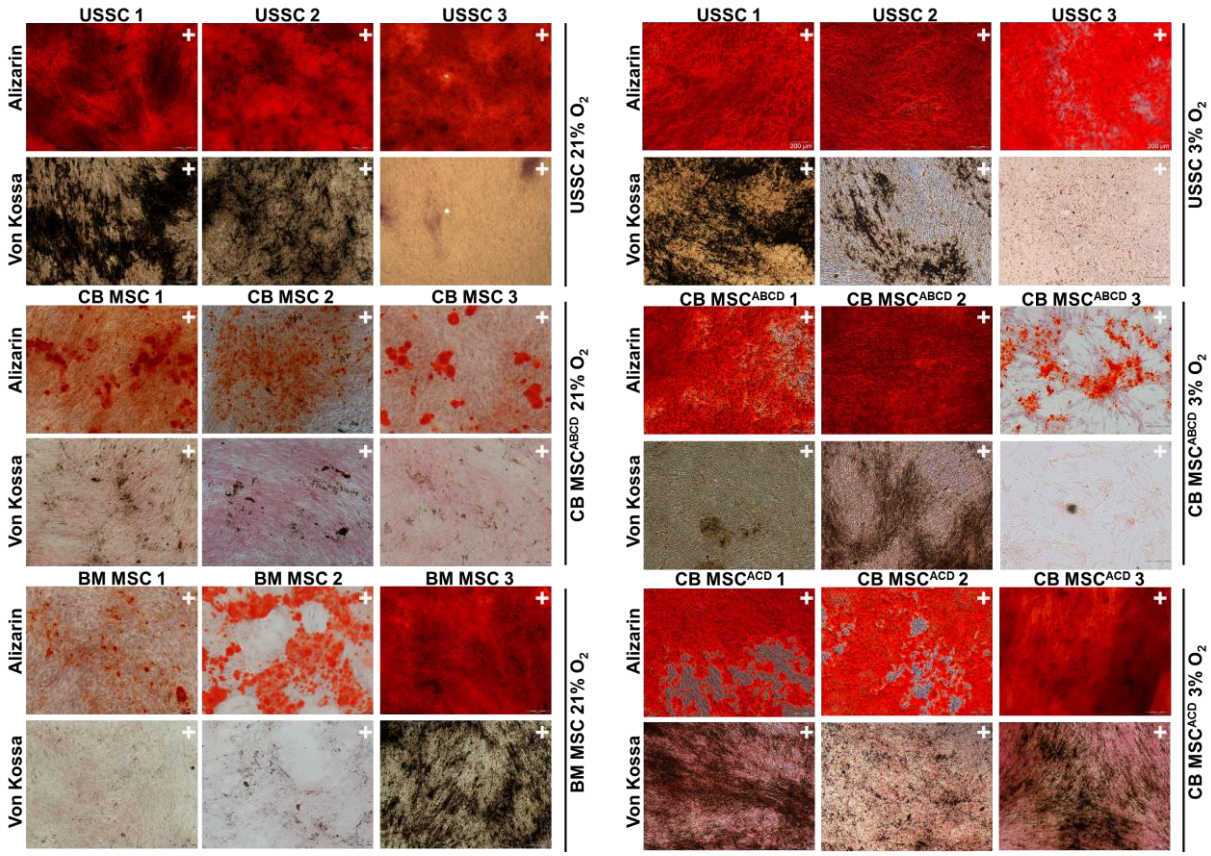

Supplemental fig. 3: Osteogenic differentiation capacity of stromal cell subtypes under normoxia and low oxygen tension. a Normoxic samples **b** Hypoxic samples. Cells were differentiated into the osteogenic lineage until day 14 and stained with Alizarin and Von Kossa staining according to standard protocols. Micrographs were acquired at room temperature with a standard Olympus CKX41 inverted microscope fitted with UPlanFLN 10x/0.3 Ph1 objective and a SIS-View FireWire camera. Pictures were taken with Cell^{D} software (Olympus Soft Imaging GmbH, Version 2.7 (Build 1224)). Single pictures (jpg. format) were then imported into Microsoft Powerpoint 2010 and combined into a single composite image. Brightness and contrast of pictures was adjusted (if needed) with the picture tools function of Microsoft Powerpoint 2010. Scale bar 200µm.

A

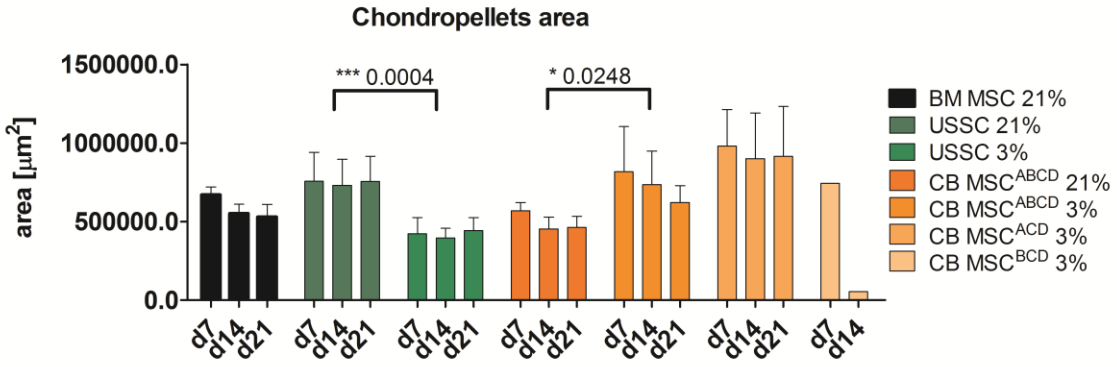

B

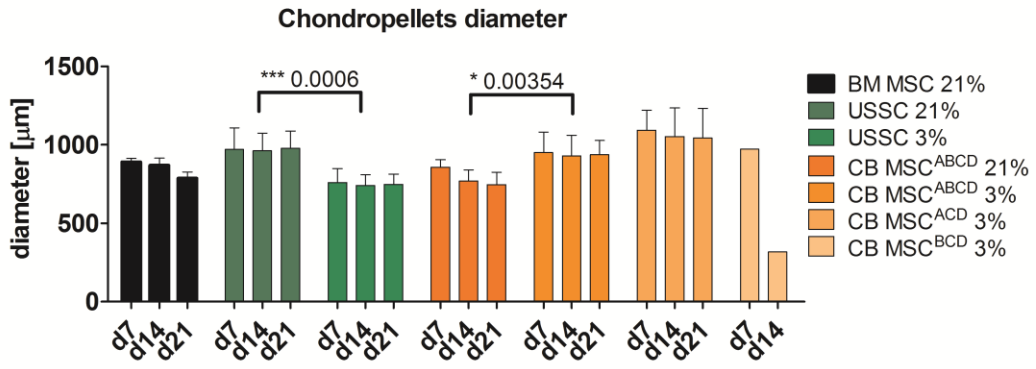

C

BM MSC 21%	area [µm²]	diameter [µm]
vs USSC 21%	ns 0.0584	ns 0.0737
vs USSC 3%	ns 0.0729	ns 0.0839
vs CB MSC^{ABCD} 21%	*** 0.0156**	ns 0.1134
vs CB MSC^{ABCD} 3%	*** 0.0332**	ns 0.0941
vs CB MSC^{ACD} 3%	**** 0.0039**	*** 0.0105**
vs CB MSC^{BCD} 3%	n.t	n.t

Supplemental figure 4. Chondrogenic differentiation potential of neonatal stromal cell subtypes under normoxia (21% O_2) and low oxygen tension (3% O_2) in comparison with adult BM MSC. **(A)** Area and diameter of chondropellets during differentiation at different time points (d7, d14, d21). The bars represent the mean ± SEM of n=5 pellets per cell line per time point. Paired t-tests were conducted with GraphPad Prism Version 5.01 to determine significance. Pellets of CB MSC^{BCD} were lost after d14 due to dissolution; significant changes upon 3% O_2 were determined in USSC and CB MSC by a paired t-test. **(B)** All neonatal stromal cell types applied here were tested for significant differences in correlation to BM MSC. At 21% O_2 and 3% O_2 no significant change was observed in USSC vs BM MSC, whereas CB MSC most likely showed a significant increase of pellet area. Pellets of CB MSC^{BCD} could not be tested (n.t.), as pellet structure was completely fragile after d14 and no chondrogenic differentiation until d21 was possible.

The *in vitro* 3D pellet culture system for chondrogenesis mimics the *in vivo* situation: Upon differentiation induction stromal cells form pre-chondroblasts resulting in growth arrest leading to condensation. Afterwards the proliferation of chondroblasts ends up in terminal differentiation and matrix deposition.

Areas and diameters of n=5 chondropellets per cell line were measured and significant changes in relation to either normoxia versus low oxygen tension or BM MSC were determined (supplemental figure. 4). All stromal cell types tested formed stable pellets in the pellet culture until d21, except for the subtype CB MSC^{BCD} lacking the HOXA-cluster (dissolution of pellet already after d14). Interestingly, a strong significant decrease in pellet area and diameter was observed in USSC under low oxygen tension compared to normoxia (supplemental figure. 4C). However, CB MSC^{ABCD} reveal as well a significant increase in pellet area and diameter supposing a different regulation of chondrogenesis at 3% O_2. The pellet area of CB MSC^{ACD} subtype strongly varied between individual cell lines due to biological heterogeneity (supplemental Fig. 2). The USSC subtype revealed nearly no condensation of the pellet over time in comparison with BM MSC and all CB MSC subtypes, supporting the individual differences observed between distinct subtypes.